Advances in Energy Research, *Vol. 5, No. 1 (2017) 13-29*
DOI: http://dx.doi.org/10.12989/eri.2017.5.1.013

Metal effects in Mn-Na_2WO_4/SiO_2 upon the conversion of methane to higher hydrocarbons

Liangguang Tang*[1], Jonghyun Choi[2], Woo Jin Lee[1], Jim Patel[1] and Ken Chiang[3]

[1]*CSIRO Energy, Private Bag 10, Clayton, VIC 3168, Australia*
[2]*The New Zealand Institute for Plant & Food Research Ltd, Waikato, New Zealand*
[3]*School of Engineering, RMIT University, Melbourne, VIC 3000, Australia*

(Received September 13, 2016, Revised April 12, 2017, Accepted April 13, 2017)

Abstract. The roles of Na, Mn, W and silica, and the synergistic effects between each metal in the Mn-Na_2WO_4/SiO_2 catalyst have been investigated for oxidative coupling of methane (OCM). The crystallisation of amorphous silica during calcination at 900℃ was promoted primarily by Na, but Mn and W also facilitated this process. The interaction between Na and Mn tended to increase the extent of conversion of Mn_3O_4 to Mn_2O_3. The formation of Na_2WO_4 was dependent on the order in which Na and W were introduced to the catalyst. The impregnation of W before Na resulted in the formation of Na_2WO_4, but this did not occur when the impregnation order was reversed. $MnWO_4$ formed in all cases where Mn and W were introduced into the silica support, regardless of the impregnation order; however, the formation of $MnWO_4$ was inhibited in the presence of Na. Of the prepared samples in which a single metal oxide was introduced to silica, only Mn/SiO_2 showed OCM activity with significant oxygen conversion, thus demonstrating the important role that Mn plays in promoting oxygen transfer in the reaction. The impregnation order of W and Na is critical for catalyst performance. The active site, which involves a combination of Na-Si-W-O, can be formed in situ when distorted WO_4^{2-} interacts with silica during the crystallisation process facilitated by Na. This can only occur if the impregnation of W occurs before Na addition, or if the two components are introduced simultaneously.

Keywords: oxidative coupling of methane; Mn-Na_2WO_4/SiO_2; synergy

1. Introduction

An increasing number of large natural gas reserves are being discovered recently. Moreover, a huge quantity of associated gas is produced during oil production, which in general is let out and/or flared. The transportation cost and environmental problems associated with gas in remoted or stranded locations have renewed the interest in the conversion of natural gas into more easily transportable liquid products such as lower emission synthetic fuels. For several decades, the oxidative coupling of methane (OCM) has been considered as an alternative route for activating methane to produce C_{2+} hydrocarbons, such as ethane and ethylene. Followed by an oligomerization process of the C_{2+} products, liquid fuels can be synthesised, which will

*Corresponding author, Ph.D., E-mail: Liangguang.Tang@csiro.au

http://www.techno-press.org/?journal=eri&subpage=7 ISSN: 2287-6316 (Print), 2287-6324 (Online)

significantly decrease the cost of transportation and environment footprint. At the same time, despite high temperature (at above 800°C) is in general required for the OCM reaction, there is a potential significantly decrease the overall energy requirement by coupling the reaction with solar energy and membrane reactor technology.

A promising catalyst for OCM reaction is Mn-Na_2WO_4/SiO_2, which was first reported by Li *et al.* (Jiang *et al.* 1993). It has remarkable thermal stability, and produces benchmark CH_4 conversions and C_2 selectivities of 20-30% and 70-80%, respectively (Chua *et al.* 2008). The structural properties and reaction mechanisms of this catalyst have been studied in detail (Jiang *et al.* 1993, Wu *et al.* 1995, Palermo *et al.* 1998, Fleischer *et al.* 2016).

Despite the attractive and reproducible catalytic performance of Mn-Na_2WO_4/SiO_2 for the OCM reaction, a consensus has not been reached regarding the nature of its active sites. Li *et al.* first suggested that reconstruction of the surface WO_4 tetrahedral units into a structure containing one W=O and three W-O-Si surface bonds was responsible for its activity (Jiang *et al.* 1993). A subsequent study proposed that the active site was indeed a distorted WO_4 tetrahedral site formed upon the electronic interaction of Na^+ ion (Wu and Li 1995). The importance of tetrahedral WO_4 was subsequently demonstrated, both experimentally and theoretically. The transition state of WO_4 interacting with CH_4 was deemed to be more stable than that of WO_6 with CH_4. As a result, WO_4 was thought to exhibit better performance for CH_4 conversion and C_2 selectivity (Ji *et al.* 2003).

A close examination of the literature revealed that synergistic interactions between individual Na, Mn and W metal ions and the SiO_2 support contribute to the observed OCM activity (Arndt *et al.* 2012). A simple combination of Na and SiO_2 shows insignificant OCM activity. However, Na promoted the transition of amorphous SiO_2 to highly crystalline α-cristobalite at lower temperatures of around 900°C (Palermo *et al.* 1998). Other alkali metals, in particular K or Rb, produced a similar effect (Palermo *et al.* 2000, Nipan *et al.* 2016).

The role of Mn in the catalyst has been extensively studied, but remains debatable. Both Mn/SiO_2 and alkali-metal-promoted Mn/SiO_2 (Jones *et al.* 1987) were reported to be active OCM catalysts under cyclic redox operations. However, Lambert reported poor OCM activity (only 23% C_2 selectivity) when Mn/SiO_2 was used in a co-feeding mode (Palermo *et al.* 1998). Li *et al.* concluded that Mn increased the mobility of the surface lattice oxygen (Wu *et al.* 1995), and Serres *et al.* (Serres *et al.* 2015) recently confirmed that Mn species act as oxygen donors to the WO_4 centres. Ji *et al.* (Ji *et al.* 2002) reported that the migration of Mn ions to the catalyst surface could be improved by the presence of Na, and that the activity was closely related to the surface Mn concentration, with the Na-O-Mn structure likely to be one of the active centres. Hou *et al.* (Hou *et al.* 2006) found that introducing Na to the Mn/SiO_2 system produced Mn_2O_3, which improved the activity and selectivity to C_2 products, and suggested that the Mn_2O_3 species were the active sites responsible for methane activation.

The W/SiO_2 combination is known to be a very poor OCM catalyst (Palermo *et al.* 1998). However, Na_2WO_4/SiO_2 has high catalytic activity for OCM conversion (Palermo *et al.* 1998), (Wu and Li 1995). Ji *et al.* (2002) suggested that there are two types of active W centres, namely tetrahedral WO_4 and octahedral WO_6, with the former proposed to be more active and selective for the OCM reaction. The replacement of W in the catalyst with Mo, Nb, V and Cr has been investigated, but W has the highest CH_4 conversion and C_2 selectivity (Mahmoodi *et al.* 2010).

It is clear that Mn, Na and W contribute to the reaction in different ways, and that intricate synergistic effects occur in the Mn-Na_2WO_4/SiO_2 catalyst. Understanding the role of each component is essential in designing a catalyst with improved performance. In this study, we systematically investigated the synergistic effects between Na, Mn, W and silica in the Mn-

Table 1 Summarize of synthesised samples

Single metal	Dual metal			Tri-metal
	0.87% Na, 2.00% Mn	0.87% Na, 3.12% W	2.00% Mn, 3.12% W	
0.87% Na/SiO_2 (*0.02 m^2/g)	$Na \rightarrow Mn/SiO_2$ (*0.16 m^2/g)	$Na \rightarrow W/SiO_2$ (*0.78 m^2/g)	$Mn \rightarrow W/SiO_2$ (*165 m^2/g)	2.0% Mn→ 5.0% Na_2WO_4/SiO_2 (*1.2 m^2/g)
2.00% Mn/SiO_2 (*170 m^2/g)	$Mn \rightarrow Na/SiO_2$ (*1.7 m^2/g)	$W \rightarrow Na/SiO_2$ (*0.07 m^2/g)	$W \rightarrow Mn/SiO_2$ (*177 m^2/g)	5.0% Na_2WO_4→ 2.0% Mn/SiO_2 (*1.3 m^2/g)
3.12% W/SiO_2 (*27.5 m^2/g)	$NaMn/SiO_2$ (*0.7 m^2/g)	Na_2WO_4/SiO_2 (*0.27 m^2/g)	WMn/SiO_2 (*180 m^2/g)	

$M_1 \rightarrow M_2/SiO_2$ represents catalyst impregnated with M_1 first and M_2 second
$M_2 \rightarrow M_1/SiO_2$ represents catalyst impregnated with M_2 first and M_1 second
M_1M_2/SiO_2 represents catalyst impregnated with M_1 and M_2 simultaneously
*: BET surface area

Na_2WO_4/SiO_2 catalyst. We impregnated a silica support with single and dual/multiple metals. In the dual/multiple case, the impregnation order of metals on the support was varied. In this case, the role of each metal and the synergistic effects between metals can be clearly revealed.

2. Experimental

2.1 Sample preparation

All samples were prepared by impregnating a silica support (Davison silica gel, 35-60 mesh) with an aqueous solution containing the desired metal salt or salts. The impregnated silica was first dried at 70℃ in a vacuum rotary evaporator for 1 h, transferred to an oven for a second stage of drying at 110℃ for 4 h, and lastly calcined at 900℃ in air for 8 h.

$NaNO_3$, $Mn(NO_3)_2 \bullet 4H_2O$ and ammonium meta tungstate hydrate were used as precursor chemicals to prepare the respective single metal Na, Mn and W-doped catalysts. The silica support was impregnated with an aqueous solution of the salt at a pre-determined concentration, and then dried and calcined.

For bimetallic catalyst synthesis, the two metals were introduced either by one or two steps of impregnation. The impregnation order was varied for catalysts synthesised in two-step impregnation. In all cases, the sample was always dried and calcined under the conditions described above after each impregnation. These samples are given the notation of $M_1 \rightarrow M_2/SiO_2$, meaning M_1 and M_2 were the first and second metals impregnated, respectively. When a sample was prepared by impregnating the two chosen metals in one step, it was labelled as M_1M_2/SiO_2. The precursors used were similar to the single metal formulation, with the exception of the co-impregnated Na and W catalyst, where $Na_2WO_4 \bullet 2H_2O$ was used.

Trimetallic catalysts were prepared by a two-step impregnation using $Mn(NO_3)_2 \bullet 4H_2O$ and $Na_2WO_4 \bullet 2H_2O$ as the precursors, with drying and calcination steps between each impregnation. The order of impregnation of $Mn(NO_3)_2$ and Na_2WO_4 was varied.

The amounts of various metal components in the different samples were fixed at 2.0 wt% Mn-5.0 wt% Na_2WO_4/SiO_2, which is widely used in the literature and proves to demonstrate superior

OCM activity. Table 1 summarizes the samples prepared for this study.

2.2 Catalyst characterization

Scanning electron microscopy (SEM) studies were carried out using a Helios NanoLab 600 (FEI). To improve visualisation of the surface, samples were coated with gold (~10 nm thick) by sputtering. The Brunauer-Emmet-Teller (BET) surface area was measured using a volumetric adsorption analyser (ASAP 2020; Micromeritics). Prior to the analysis, each sample was out-gassed under vacuum at 350°C overnight to remove any pre-adsorbed gaseous species.

X-ray diffraction (XRD) analysis was performed on a Phillips DW 1130 with a radiation source of Cu Kα (λ=1.5406 Å), operated at 40 kV and 25 mA. Diffractograms were recorded with a step size of 0.02° and at a scanning speed of 2°/min in a range of 2θ from 5-80°. Samples were mounted on aluminium plates and measured at room temperature.

Temperature-programmed reduction (TPR) studies were conducted in an AutoChem 2950HP analyser (Micrometric). In a typical analysis, a 100-mg sample was first dried under a flow of argon at 110℃ for 1 h and then cooled to 50℃. The supply of argon was stopped and a 10% H_2/Ar gas mixture was allowed to flow at a rate of 50 ml/min. The sample was then heated at a temperature ramp rate of 5℃/min to 850°C, and held at this temperature for 30 min. The consumption of H_2 was monitored by means of a thermal conductivity detector.

X-ray photoelectron spectroscopy (XPS) measurements were performed with an ESCALAB250Xi (Thermo Scientific, United Kingdom) with a mono-chromated Al Kα source (1486.68 eV). The reported values of binding energy in all spectra were calibrated with respect to the Si 2p line at 103.5 eV. Surface compositions were calculated from peak areas using the sensitivity factors of the spectrometer.

2.3 OCM activity testing

OCM activity was assessed in a fixed-bed reactor under atmosphere pressure. In each experiment, 100 mg of sample was first diluted with 400 mg of quartz powder and packed inside a 6-mm ID quartz reactor. The catalyst bed was held in position by quartz wool packing above and immediately below the catalyst bed. Before the reaction commenced, each sample was heated to the desired temperature inside the reactor under a flow of 4%O_2/Ar. Argon was then purged through the catalyst bed for 30 min to remove any residual oxygen. The reaction was commenced by introducing a flow (100 mL/min) of CH_4/O_2/Ar at a volumetric ratio of 5:1:44 through the catalyst bed. The catalyst bed temperature was maintained at 900℃ in all experiments. Since OCM is an exothermic reaction, the low concentration of CH_4 and O_2 in the feeding gas, along with the diluted catalyst sample, helped to prevent the development of a large temperature gradient across the catalyst bed and the temperature increase in the bed was less than 3℃ for all tests. It was emphasized here that the most common temperature range for OCM reaction reported is based on the required feed-gas temperature and is in the range of 750-850℃. The temperature increase in the catalyst bed were in general not reported in the literature, and it is hard to compare the reaction temperature reported with the bed temperature in our current studies. Trial runs have confirmed up to 200℃ increase of bed temperature for the most active catalyst if no feeding gas and catalyst bed dilution, which suggested that the 900℃ bed temperature adopted in the current study is in a similar temperature range as reported in the literature. The temperature spike has been reported recently (Noon *et al.* 2013). The outlet gas composition was analysed by an online micro gas

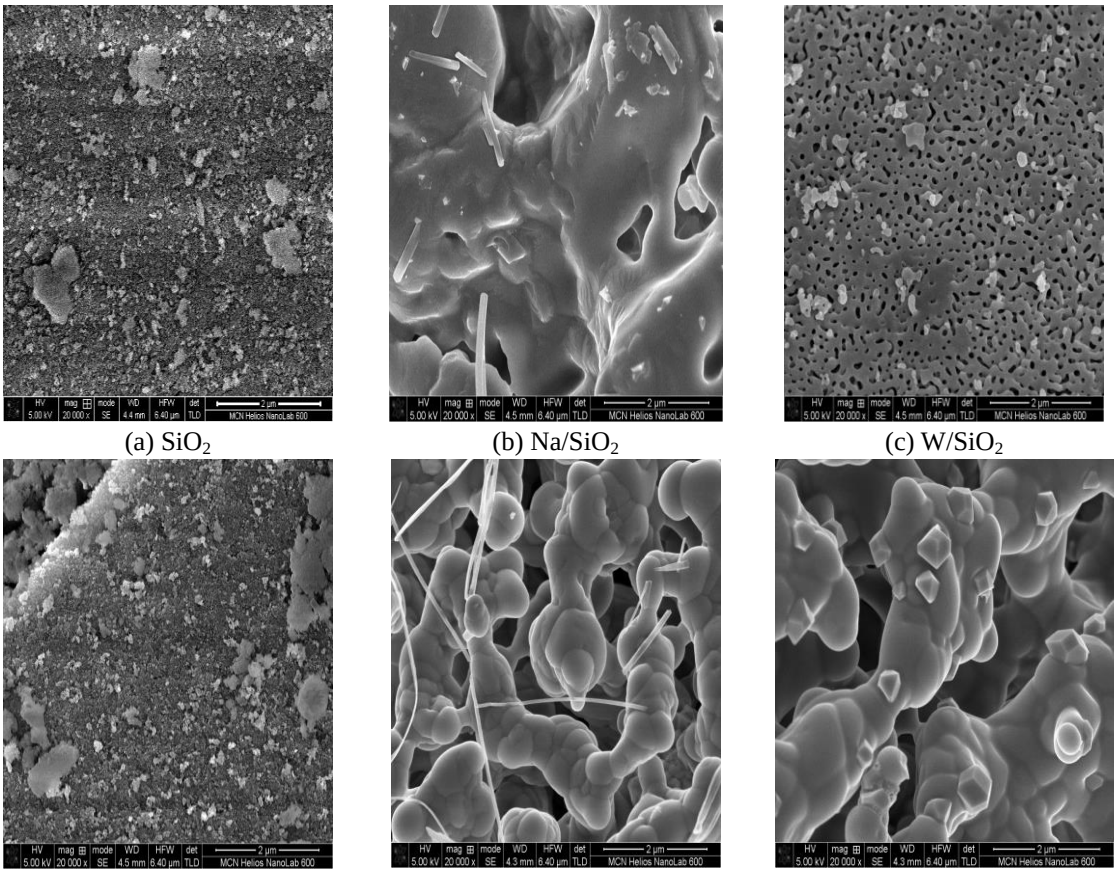

(a) SiO_2 (b) Na/SiO_2 (c) W/SiO_2

(d) Mn/SiO_2 (e) Na_2WO_4/SiO_2 (f) $Mn \rightarrow Na_2WO_4/SiO_2$

Fig. 1 Scanning electron microscopy of samples. All samples were calcined at 900℃ for 8 h

chromatograph (Varian 490) with dual thermal conductivity detectors. All conversions reported were determined when the reaction reached a steady state, typically after 2 h time-on-stream.

3. Results

3.1 The effect of metal(s) on sample morphology

The silica support calcined at 900℃ was comprised primarily of particles between 15-30 nm in size, and the primary particles had a tendency to form larger particles (Fig. 1(a)). The support retained a surface area of 180 m^2/g after calcination. The addition of Na and W changed the support morphology significantly. The introduction of Na caused the SiO_2 particles to fuse, leaving the final structure with no clear particle boundaries. The edge of the fused particles had a regular crystalline shape (Fig. 1(b)). In addition, the BET surface area of Na/SiO_2 was 0.02 m^2/g, which is much lower than the original silica material. In contrast, the material produced by introduction of W to SiO_2 retained a macroporous structure (Fig. 1(c)) and had a surface area of 27.5 m^2/g. Manganese had little effect on the morphology of the SiO_2 (Fig. 1(d)), and the surface area

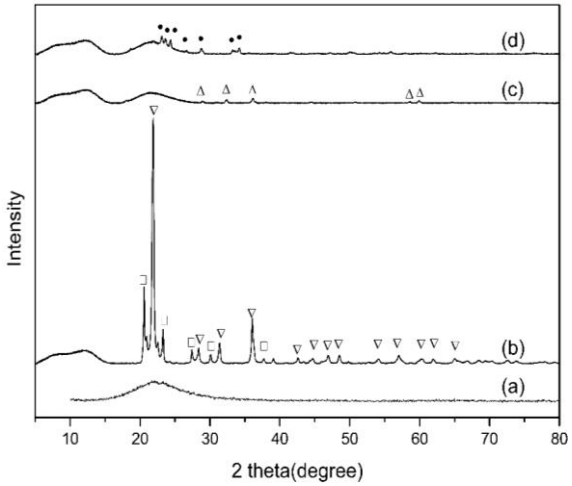

Fig. 2 X-ray diffraction analysis of unsupported and single metal supported on SiO_2. (a) SiO_2, (b) Na/SiO_2, (c) Mn/SiO_2, (d) W/SiO_2. ▽:α-cristobalite, □:Tridymite, Δ:Mn_3O_4, ●:WO_3

(170 m^2/g) of Mn/SiO_2 was similar to that of fresh silica.

Similar to Na/SiO_2, the Na_2WO_4/SiO_2 showed a fused morphology with a well-defined macroporous structure, and particle boundaries could be identified (Fig. 1(e)). The trimetallic formulation, $Mn \rightarrow Na_2WO_4/SiO_2$, produced a similar morphology to Na_2WO_4/SiO_2. However, small particles with regular crystalline shape were observed at the surface (Fig. 1(f)). A surface area of 1.2 m^2/g was measured for $Mn \rightarrow Na_2WO_4/SiO_2$.

3.2 XRD analysis

XRD analysis of the calcined SiO_2 (Fig. 2(a)) showed a broad peak at ca. 2θ=22°, suggesting the material is still amorphous. Theoretically, calcination at 900℃ is unlikely to induce any crystal phase change (Palermo *et al.* 1998). However, when Na was introduced to SiO_2, calcination at 900℃ produced α-cristobalite and a structure similar α-tridymite (Fig. 2(b)), which suggests that crystallisation of amorphous SiO_2 increases in the presence of sodium. In addition, the absence of diffraction peaks related to sodium species suggests that sodium could be well diffused into and dispersed throughout the support.

Unlike Na, Mn and W did not change the crystallinity of silica upon calcination. The base silica material remained in an amorphous form, as confirmed by the broad XRD peak at ca. 2θ=22° (Fig. 2(c) and 2(d)). The relatively weak diffraction peaks at 2θ=28.8°, 32.3° and 36.1° for the Mn/SiO_2 sample (Fig. 2(c)) can be indexed to the (112), (103) and (211) planes of the tetragonal Mn_3O_4 phase (Gao *et al.* 2011), suggesting that manganese oxide was in the form of Mn_3O_4. The major diffraction peaks at 2θ=23.2°, 23.68° and 24.4° shown in Fig. 2(d) were observed in the W/SiO_2, and these can be indexed to reflections from the (001), (020) and (200) planes of monoclinic WO_3 (Senthil and Yong 2007). The intensity of the XRD peaks attributed to crystalline manganese oxide and tungsten oxide were very low, suggesting that incorporated oxides could be either highly amorphous or highly dispersed throughout the support.

A new peak at 2θ=32.9° was identified in both $Na \rightarrow Mn/SiO_2$ (Fig. 3(a)) and $Mn \rightarrow Na/SiO_2$ (Fig. 3(b)), and this can be assigned to Mn_2O_3 (Hou *et al.* 2006). The results suggest that Mn_2O_3 is

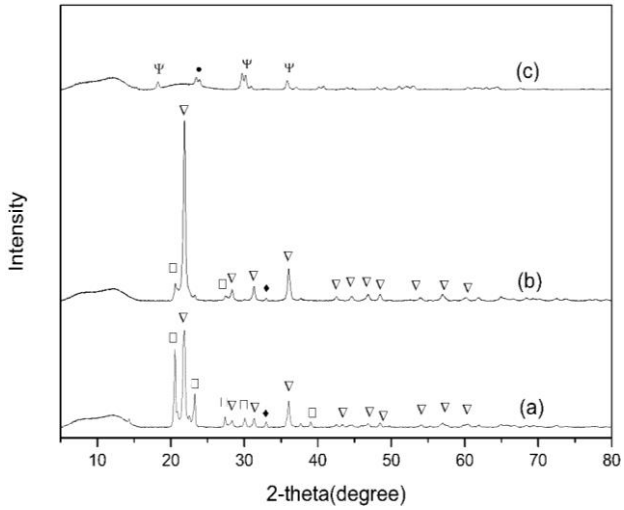

Fig. 3 X-ray diffraction analysis of dual metals supported on SiO_2. (a) Na→Mn/SiO_2, (b) Mn→Na/SiO_2, (c) MnW/SiO_2. ▽:α-cristobalite, □:Tridymite, ◆:Mn_2O_3, ●:WO_3, Ψ:$MnWO_4$

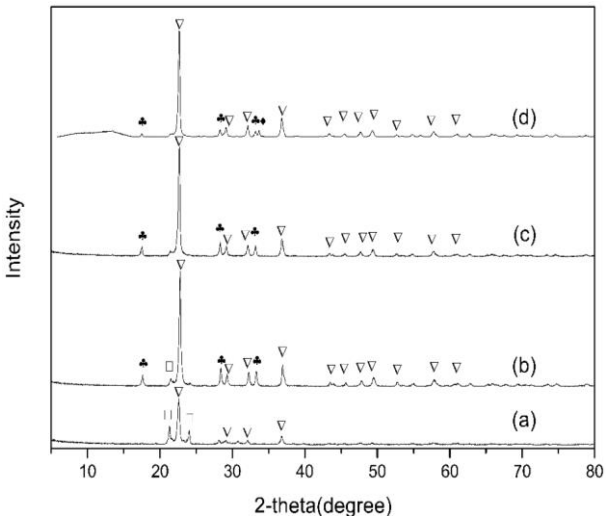

Fig. 4 X-ray diffraction analysis of Na and W supported on SiO_2. (a) Na→W/SiO_2, (b) W→Na/SiO_2, (c) Na_2WO_4/SiO_2, (d) Mn→Na_2WO_4/SiO_2. ▽:α-cristobalite, □:Tridymite, ◆:Mn_2O_3, ♣:Na_2WO_4

preferentially formed in the presence of sodium. In addition, a close examination of the crystalline structure of silica in Na→Mn/SiO_2 and Mn→Na/SiO_2 revealed a subtle difference. For Mn→Na/SiO_2, the tridymite peaks became less intense and the α-cristobalite peak increased in intensity compared with Na→Mn/SiO_2. NaMn/SiO_2 had the same profile as Mn→Na/SiO_2, and is not shown here.

The order of impregnation significantly affected the crystallinity of the materials when both Na and W were present. Peaks originating from tungsten species were not identified for Na→W/SiO_2, as shown in Fig. 4(a). However, when the impregnation order was reversed (W→Na/SiO_2, Fig. 4(b)) or when Na and W were introduced simultaneously (Fig. 4(c)), the presence of Na_2WO_4

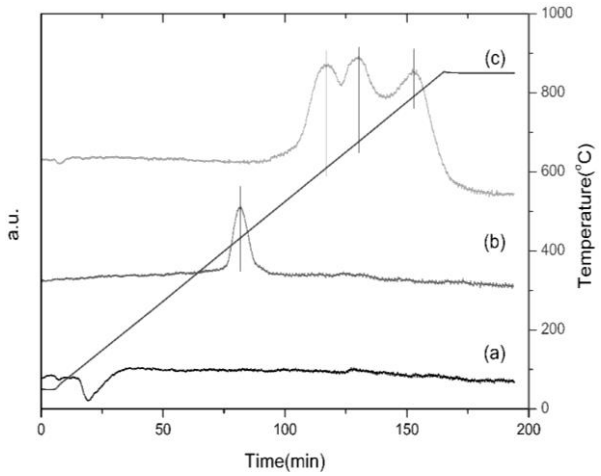

Fig. 5 Reduction profile of single metal supported on SiO_2. (a) Na/SiO_2, (b) Mn/SiO_2, (c) W/SiO_2

was identified, as suggested by peaks at 2θ=16.8° and 32.5°. Similar to the Na and Mn system, the order of impregnation for Na and W had a subtle effect on the crystalline structure of SiO_2. Compared to $Na\rightarrow W/SiO_2$, an increase of α-cristobalite peaks were observed in $W\rightarrow Na/SiO_2$ and Na_2WO_4/SiO_2, while α-tridymite peaks disappeared.

The interaction between Mn-W resulted in new peaks at 2θ=18.3, 29.8 and 30.2° (Fig. 3(c)), which can be ascribed to the $MnWO_4$ phase (Ji *et al.* 2002). However, these peaks were not observed in the trimetallic system, where Mn_2O_3 and Na_2WO_4 phases were identified (Fig. 4(d)), suggesting that Na can inhibit the formation of $MnWO_4$.

3.3 Reduction behaviour from TPR studies

No reduction peaks were observed for Na/SiO_2, as shown in Fig. 5(a). The reduction profile of Mn/SiO_2 included one dominant peak at ca. 434°C (Fig. 5(b)), which can be assigned to the reduction of Mn_3O_4 to MnO. Reduction to zero valent Mn is not expected under the current reductive conditions, since MnO cannot be readily reduced by H_2 below 1000℃ (Ren *et al.* 2011). The W/SiO_2 showed three reduction peaks at 611, 676 and 790°C, as shown in Fig. 5(c). The stepwise reduction of bulk WO_3 to zero valent tungsten has been suggested to proceed in the order of $WO_3(VI)\rightarrow W_{20}O_{58}(V,VI)\rightarrow WO_2(IV)\rightarrow W(0)$, which gives rise to three distinct reductions at 670, 715 and 885°C (Zhao *et al.* 2009). The W/SiO_2 catalyst could likely follow the similar three-stage reduction pathway of bulk WO_3, but the reaction seems occur at lower reduction temperature due to the interaction between WO_3 and the silica support.

The reduction of $Mn\rightarrow Na/SiO_2$ was characterised by two peaks at 465 and 646°C (Fig. 6(a)), which can be ascribed to the two-step reduction of $Mn_2O_3\rightarrow Mn_3O_4\rightarrow MnO$. Both the TPR and XRD results suggest a phase transformation from Mn_3O_4 to Mn_2O_3 in the presence of Na. It also appears that the order of impregnation of Na and Mn does not affect the reduction profile of the resultant samples. Both $Na\rightarrow Mn/SiO_2$ and $MnNa/SiO_2$ had a similar reduction profile to $Mn\rightarrow Na/SiO_2$ (result not shown).

The TPR of $Na\rightarrow W/SiO_2$ showed two reduction peaks at 575 and 739℃, as shown in Fig. 6(b). As suggested by Zhao *et al.* the high-temperature reduction peak and the weaker low-temperature

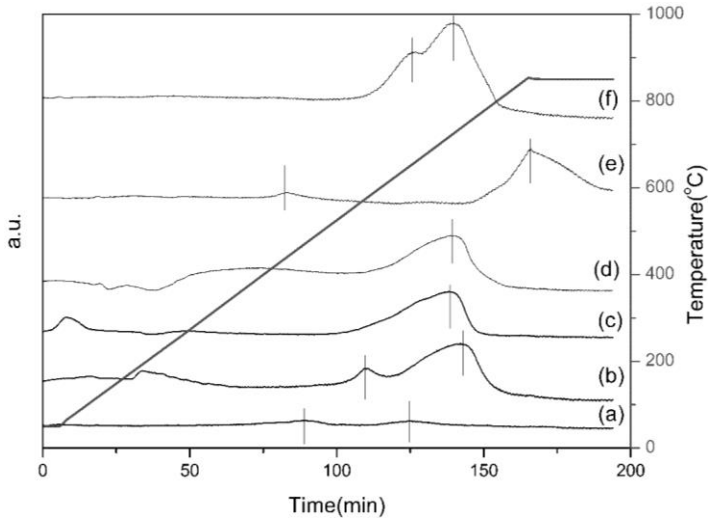

Fig. 6 Reduction profile of multiple metals supported on SiO_2. (a) Mn→Na/SiO_2, (b) Na→W/SiO_2, (c) W→Na/SiO_2, (d) Na_2WO_4/SiO_2, (e) MnW/SiO_2, (f) Mn→Na_2WO_4/SiO_2

peak could be attributed to the reduction of WO_3 and octahedral W species, respectively (Zhao *et al.* 2009). The differences in the reduction profiles for Na→W/SiO_2 and W/SiO_2 suggested that W could have interacted differently with α–cristobalite and amorphous SiO_2, but it is not yet clear how this affects the reduction profile. Both W→Na/SiO_2 (Fig. 6(c)) and Na_2WO_4/SiO_2 (Fig. 6(d)) showed the same reduction profile, with only one dominant peak at 719℃ that was ascribed to the reduction of Na_2WO_4 species. Compared with Na→W/SiO_2, the reduction peak of both W→Na/SiO_2 and Na_2WO_4/SiO_2 shifted to 20℃ lower, and the low-temperature peak was missing.

The reduction profiles of Mn→W/SiO_2, W→Mn/SiO_2 and MnW/SiO_2 were similar; therefore, only the reduction profile of MnW/SiO_2 is provided in Fig. 6(e). A significant peak at ca. 850°C and a minor peak at 436℃ were present. The high-temperature peak, which was not observed in any previous results, can be ascribed to the reduction of $WMnO_4$ species as detected in XRD. The small peak is possibly due to the reduction of Mn species.

Two reduction peaks at 646 and 719°C were observed in the trimetallic catalyst (Fig. 6(f)). Because these temperatures agree well with those already discussed, they can be ascribed to the reductions of Na_2WO_4 and Mn_2O_3, respectively. No high-temperature peak for the $WMnO_4$ phase was observed, which confirms the inhibiting effect of Na in forming the $WMnO_4$ phase, as observed in the XRD analysis.

3.4 XPS results

Tables 2 and 3 list the observed binding energies and near-surface composition of selected samples. As shown in Table 2, in addition to the adventitious carbon at ca. 284.9 eV that was detected in all samples, a second carbon species with a C 1s binding energy of 289.5±0.5 eV was detected on the surface of all Na-containing samples. It is believed that the Na_2CO_3 that formed upon calcination contributed significantly to the evolution of this peak. The carbon species from Mn and W were not expected. This is because $MnCO_3$ can easily decompose at 200℃, and would not survive under the current calcination temperature. The formation of tungsten carbide, on the

Table 2 Observed binding energies (eV) of selected samples

Samples	O(1s)		C(1s)		Na(1s)	Mn(2p)	W(4f)
	SiO_2	MOx	Adventitious	CO_3^{2-}			
SiO_2	532.7	-	284.9	-	-	-	-
Na/SiO_2	532.7	531.0	285.0	290.0	1071.7	-	-
Mn/SiO_2	533.3	530.4	284.9	-	-	641.9	-
W/SiO_2	533.2	530.8	285.0	-	-	-	36.0
$Na\rightarrow W/SiO_2$	532.7	530.4	284.9	289.1	1071.5	-	35.5
$W\rightarrow Na/SiO_2$	532.6	530.5	284.9	289.4	1071.5	-	35.4
Na_2WO_4/SiO_2	532.6	530.4	284.9	289.5	1071.5	-	35.5
$Na\rightarrow Mn/SiO_2$	532.5	530.5	284.9	289.2	1071.7	642.1	-
WMn/SiO_2	532.8	530.4	284.8	-	-	641.4	35.2
$Mn\rightarrow Na_2WO_4/SiO_2$	532.5	530.4	284.9	289.3	1071.6	641.6	35.4

MOx represents the metal oxides, except for SiO_2

Table 3 Near-surface elemental composition (a.t. %) of selected samples

	Si(2p)	O(1s)		C(1s)		Na	Mn	W
Samples		SiO_2	MOx	Adventitious	CO_3^{2-}			
SiO_2	63.2	36.1		0.7				
Na/SiO_2	27.6	51.1	5.2	5.4	3.3	7.4		
Mn/SiO_2	35.9	61.4	0.8	1.7			0.2	
W/SiO_2	34.4	59.8	1.9	3.5				0.4
$Na\rightarrow W/SiO_2$	27.3	44.8	11.3	7.0	0.7	5.0		3.1
$W\rightarrow Na/SiO_2$	30.6	50.4	5.8	6.9	1.2	3.7		0.6
Na_2WO_4/SiO_2	30.6	51.1	5.7	6.7	1.2	3.0		0.8
$Na\rightarrow Mn/SiO_2$	30.6	47.8	7.5	6.9	0.7	5.0	1.5	
WMn/SiO_2	35.3	62.5		1.9			0.2	0.1
$Mn\rightarrow Na_2WO_4/SiO_2$	28.9	47.4	7.8	8.0	1.2	4.8	1.0	0.8

other hand, requires temperature above 1400℃.

The binding energy of O (1s) for SiO_2 was 532.7 eV. When different metal oxides were impregnated on the support, several oxygen-containing species (e.g., MnOx, WO_4^{2-}, WO_3, CO_3^{2-}) were present, resulting in the appearance of new O(1s) peaks in a binding energy range of 530.5±0.5 eV.

The near-surface compositions of the metal-doped samples had higher oxygen concentrations than the SiO_2 support (Table 3). The surface oxygen in SiO_2 was 36.1%; this value increased to 61.4 and 59.8% in Mn/SiO_2 and W/SiO_2, respectively. The Na/W atomic ratios measured for $W\rightarrow Na/SiO_2$, Na_2WO_4/SiO_2 and $Mn/Na_2WO_4/SiO_2$ were greater than 2. This suggests that only a small portion of Na is in the form of Na_2WO_4, while a significant amount of surface sodium could be present as Na_2CO_3 or Na_2O/Na_2O_2. This observation also agrees with the results reported by Zhang *et al.* (Zhang *et al.* 2006). The Na/W ratio for $Na\rightarrow W/SiO_2$, on the other hand, was only 1.6. The enrichment of tungsten species on the surface of $Na\rightarrow W/SiO_2$ suggests that the

Table 4 Oxidative coupling of methane catalytic performance of different samples

Samples	CH_4 conversion (%)	O_2 conversion (%)	C_2 selectivity (%)	C_2 yield (%)	C_2H_4/C_2H_6 ratio
Na/SiO_2	1.9	8.4	62.5	1.2	0.33
Mn/SiO_2	15.3	84.9	47.9	7.3	1.48
W/SiO_2	10.9	53.6	17.5	1.9	0.50
$NaMn/SiO_2$	17.2	31.3	39.5	6.8	0.72
$Na→Mn/SiO_2$	7.92	32.2	59.7	4.7	0.60
$Mn→Na/SiO_2$	14.5	42.8	56.8	8.2	0.68
Na_2WO_4/SiO_2	19.9	71.3	73.6	14.6	1.83
$Na→W/SiO_2$	7.4	25.1	65.1	4.8	0.62
$W→Na/SiO_2$	23.4	98.5	73.4	17.2	2.13
WMn/SiO_2	18.7	96.2	41.1	7.7	1.47
$W→Mn/SiO_2$	15.5	91.0	53.5	8.3	1.51
$Mn→W/SiO_2$	14.3	88.7	35.3	5.0	1.04
$Mn→Na_2WO_4/SiO_2$	26.1	100.0	69.3	18.1	2.46
$Na_2WO_4→Mn/SiO_2$	26.0	100.0	69.2	18.0	2.36

T: 900℃, CH_4:O_2:Ar=5:1:44, Total flow rate: 100 ml/min, Mass: 0.1 g catalyst mixed with 0.4 g quartz

interaction between Na and W is low, and that tungsten most probably existed as isolated WO_3 centres.

The surface concentration of Na was 7.4% in Na/SiO_2. This was higher than the average bulk composition, suggesting that Na was enriched on the surface. The surface concentrations for Mn and W were only 0.2 and 0.4% in Mn/SiO_2 and W/SiO_2, indicating that both metals diffused into the bulk of the support and were not enriched on the surface. However, the surface concentration of W increased to 0.6% in the presence of sodium ($W→Na/SiO_2$), and this could be due to two reasons. One reason is that Na helps the migration of Mn and W to the surface. The other is the Na addition causes a lower surface, resulting in a higher surface concentration of Mn and W.

3.5 OCM activity

The catalytic performance of different samples is provided in Table 4. Both Na/SiO_2 and W/SiO_2 showed very poor OCM activity, with C_2 yields less than 2%. This agrees with previous studies (Palermo *et al.* 1998). On the other hand, Mn/SiO_2 showed some OCM activity, with a CH_4 conversion of 15.3% and a C_2 selectivity of 47.9%. An O_2 conversion of 84.9% was also observed for Mn/SiO_2.

Both $Mn→Na/SiO_2$ and $NaMn/SiO_2$ gave similar C_2 yields to Mn/SiO_2, but $Na→Mn/SiO_2$ was less active. However, the O_2 conversion for these three samples was significantly lower than that for Mn/SiO_2, with a maximum O_2 conversion of only 42.8% for $Mn→Na/SiO_2$. The impregnation order of Na and W significantly influenced OCM activity. $Na→W/SiO_2$ showed poor OCM activity, with a CH_4 conversion of 7.4% and a C_2 selectivity of 65.1%, resulting in a C_2 yield of 4.8%. However, OCM activity dramatically improved for $W→Na/SiO_2$ and Na_2WO_4/SiO_2, with a C_2 yield of 17.2 and 14.6%, respectively. The impregnation order of Mn and W showed little effect on OCM activity compared with Mn/SiO_2. However, the O_2 conversion for Mn-W samples

was high, within a range of 88.7-96.2%.

Irrespective of the impregnation order of Mn and Na_2WO_4, both trimetallic catalysts gave the highest C_2 yield (18.0 and 18.1%) with 100% O_2 conversion under the testing conditions. Although the optimization of the experimental conditions to further improve C_2 yield was not carried out, the results given here are generally in line with those of earlier studies (Wu *et al.* 1995, Hou *et al.* 2006, Zhang *et al.* 2006, Czuprat *et al.* 2010).

4. Discussion

Our results clearly demonstrate that each component in the Mn-Na_2WO_4/SiO_2 system plays a unique role, and that strong metal-metal and metal-support synergies exist. In particular, the interaction between sodium, tungsten and the silica support are critical for an OCM catalyst to function efficiently.

It is reported that silica starts transform into tridymite at 870℃, and tridymite transforms into α-cristobalite at 1470℃ (Sharma 1997). α-Cristobalite phase was detected when Na/SiO_2 was calcined under 900℃, suggesting that the presence of Na is essential for the crystallisation of SiO_2 at low temperature (Palermo *et al.* 1998). The accelerated crystallisation of amorphous SiO_2 into the cristobalite phase at temperatures below 1000℃ has also been reported when the SiO_2 surface is coated with silver and gold, where these metal can concentrate heat and turn themselves into hot spots to facilitate phase transformation (Pol *et al.* 2003).

The impregnation order of Na and Mn/W has a subtle effect on SiO_2 crystalline structure. When Na was impregnated first, followed by either Mn or W, the XRD patterns of corresponding samples showed peaks ascribed to α-cristobalite (e.g., 2θ=21.9°) and tridymite (e.g., 2θ=20.6 and 23.3°), which was similar to the XRD profile of Na/SiO_2. However, the tridymite peak was not observed in Mn→Na/SiO_2, W→Na/SiO_2, $NaMn/SiO_2$ or NaW/SiO_2. The XRD results suggested that tungsten oxide and manganese oxide did not directly contribute to the silica crystallisation process. However, the presence of these oxides with sodium did improve the crystallisation of silica. When the phase transformation of silica occurred first (by impregnation with Na), the improvement of the silica crystallisation process in the presence of other metal oxides ceased. This confirms that synergistic effects exist between Mn/W and Na.

Because Na/SiO_2 showed very poor OCM activity, it can be conclude that the active site of the catalyst is not directly related to sodium species, such as $Na_2CO_3/Na_2O_2/Na_2O$. A CH_4 conversion of 15.3% and a C_2 selectivity of 50% was obtained for 2.0 wt% Mn/SiO_2, which is close to the C_2H_4 yield of 4.3% reported by Palermo *et al.* (Palermo *et al.* 1998). Upon the introduction of sodium to Mn/SiO_2, the manganese was transformed from Mn_3O_4 to Mn_2O_3. However, little improvement in OCM activity was observed.

The role of Mn in the OCM reaction has been a matter of debate. Jones *et al.* (Jones *et al.* 1987) conducted a series of redox experiments, reporting an improvement of C_2 selectivity upon addition of Na to the manganese-silica system. A CH_4 conversion of 12% and a C_2 selectivity of 88% were obtained for 10 wt% Mn/1.7 wt% Na/SiO_2. It was ascribed the beneficial effects to the increase in surface basicity, the unique sodium-manganese interaction and the reduced surface area. The beneficial effect of sodium addition to Mn/SiO_2 was not observed in the current study, which could be due to the following reasons. First, a 2 wt% loading of Mn was used in this study, which is low compared with the Mn loading of 10 wt% adopted in Jones *et al.*'s work. Second, Jones *et al.* adopted a cyclic redox approach to assess catalytic activity, while methane and oxygen were

co-fed to the reaction in this study. In the redox model, an active and efficient participation of bulk lattice oxygen in the catalyst for the coupling reaction is critical (Wang *et al.* 1995). As a result, a higher metal loading and a lower gas hourly space velocity (GHSV) (i.e., 860 h^{-1}) were adopted in Jones *et al.*'s study. However, when methane and molecular oxygen are co-fed to the catalyst, the contribution from lattice oxygen in the catalyst is minimal. As a result, a lower metal loading and a higher GHSV (i.e., 9700 h^{-1}) were applied in this study.

Na-O-Mn was regarded as the active centre by Wang *et al*. because Mn-Na_2WO_4/SiO_2, Mn-Na_2WO_4/MgO and $NaMnO_4$/MgO showed similar catalytic performance after 10 h time-on-stream (Wang *et al.* 1995). Their work showed the 5.0 wt%$NaMnO_4$/MgO that contained no tungsten species gave a CH_4 conversion of 5% and a C_2 selectivity around 80% at steady state, which was far lower than the initial activity of Mn-Na_2WO_4/SiO_2, with a CH_4 conversion of 20% and a C_2 selectivity of over 80%. In this case, the low activity of 5.0 wt%$NaMnO_4$/MgO cannot support the argument that Na-O-Mn is the active centre. The lack of change in OCM activity in response to the impregnation order of Na and Mn also suggests that the interaction between Na and Mn is less important for CH_4 activation.

Based on all effective catalysts reported in the literature containing Mn_2O_3 as a required species, Hou *et al.* (Hou *et al.* 2006) suggested that Mn_2O_3 was the active site, or at least contributed directly to the formation of the active sites. The redox cycles between Mn^{3+} (Mn_2O_3) and $Mn^{\delta+}$ ($2<=\delta<3$), which depict the role of Mn in facilitating the transfer of oxygen between the gas phase and lattice, were proposed to be the main mechanism controlling the OCM reaction.

Manganese oxide is an active catalyst in several oxidation and reduction reactions, and has been used for the oxidation of methane and carbon monoxide, and the selective reduction of nitrobenzene (Stobbe *et al.* 1999). Moreover, the application of manganese oxide as an oxygen-storage component for a three-way catalyst has been proposed, and the oxygen adsorption and desorption behaviour of manganese oxide has been demonstrated as superior to that of cerium oxide (Chang and McCarty 1996). Kou *et al.* suggest that the manganese ion tends to maintain a 4-coordinated, square-planar geometry by making two axial oxygens empty, thus acting as a good oxygen releaser (Kou *et al.* 1998).

In this study, reasonable CH_4 activation was observed for 2.0 wt% Mn/SiO_2. However, a salient feature observed for Mn/SiO_2 was its high oxygen conversion (85%), which indicates that manganese oxide supported on SiO_2 has high oxygen activation ability. Based on the previous discussion, we propose that the manganese oxide has dual functions: it has some functions for CH_4 activation, while its main role is related to O_2 activation. It may improve exchanges between the gas-phase molecular oxygen and the lattice oxygen in the solid phase, most possibly through a redox route involving Mn^{3+}/Mn^{2+}(Gordienko *et al.* 2016). However, the oxygen activation ability was decreased for Na-doped Mn/SiO_2, which was evident from the low oxygen conversion for all three Na-Mn supported samples.

W/SiO_2 showed very poor OCM activity in terms of C_2 yield. The XRD suggested that the main phase is amorphous SiO_2 and WO_3, which consists of octahedral WO_6 arranged in various sharing configurations (corners, edges and planes). The surface elemental W/O ratio given by XPS was 0.18, which confirmed the octahedral structure. Octahedron WO_6 is suggested to have inferior OCM activity (Ji *et al.* 2003).

Recently, Simon *et al.* (Simon *et al.* 2011) and Hou *et al.* (Hou *et al.* 2006) reported the presence of $MnWO_4$ phase in Mn-Na_2WO_4/SiO_2 catalyst, and this was confirmed in our XRD analysis of W-Mn supported on SiO_2. Since the W-Mn supported on SiO_2 showed similar OCM activities as Mn/SiO_2, we suggest that the combination of W and Mn is not directly related to the

Table 5 Effect of different supports on oxidative coupling of methane performance

Catalyst	CH_4 conversion (%)	C_2 selectivity (%)	C_2 yield (%)
2.0%Mn/5%Na_2WO_4/Al_2O_3[(a)]	15.9	45.5	7.2
Na_2WO_4/MgO[(b)]	3.6	58.0	2.1
5%Na_2WO_4/ cristobalite[(c)]	8.0	54.0	4.3
2.0%Mn/5%Na_2WO_4/MgO[(d)]	5.4	64.9	3.2

(a) T: 900℃, CH_4:O_2:Ar=5:1:44, Total flow rate: 100 ml/min, Mass: 0.1 g catalyst mixed with 0.4 g quartz
(b) T: 800℃, CH_4:O_2=670:90(torr), Total flow: 115 ml/min, Mass: 1.0 ml (Wang *et al.* 1995)
(c): T: 850℃, CH_4:O_2=4.5:1, Total flow: 18 ml/min; Mass: 0.4 g (Palermo *et al.* 1998)
(d): T: 800℃, CH_4:O_2=4:1, Total flow: 100 ml/min; Mass: 0.05 g (Elkins and Hagelin-Weaver 2015)

active centre for CH_4 activation. However, high oxygen conversion was observed for the samples containing W and Mn. For example, the oxygen conversion was 96.2% for WMn/SiO_2. This indicates that tungsten can maintain or improve the oxygen transfer ability of manganese during the reaction, which could be due to the reaction involving electron transfer between a W^{5+} and nearby Mn^{3+}, as suggested by Elkins *et al.* (Elkins and Hagelin-Weaver 2015).

The $MnWO_4$ phase was not observed in the trimetallic system, which suggests that the presence of Na could inhibit its formation. Ji *et al.* also reported the absence of $MnWO_4$ when the Na content was increased to 0.7% (Ji *et al.* 2003). This excludes $MnWO_4$ as the active centre for OCM reaction.

The impregnation order of Na and W significantly affected the structure and OCM performance of samples. Na→W/SiO_2 gave poor OCM activity, with a C_2 yield of only 4.8%, while a significant increase in C_2 yield of up to 17.2% was observed for W→Na/SiO_2; this is comparable to those from trimetallic samples. Na_2WO_4/SiO_2 also improved OCM activity, with a C_2 yield of 14.6%. In both cases, an Na_2WO_4 phase was identified from XRD analysis. The results suggest that the interaction between Na and W is crucial for an efficient catalyst.

As shown in Table 4, the oxygen conversion in the three metal catalyst is 100%, which suggested that under certain conditions, the catalyst may be limited by reoxidation rather than CH_4 activation. The oxygen activation which is related to Na-O-Mn combination is not clear at this stage and further work needs to be done.

To investigate the effect of the supports on OCM activity, the trimetals were also supported on alumina in the current study and the OCM activity was evaluated. Activity data of some other supports (e.g., MgO, cristobalite) was taken from literature. Table 5 summarised all the available activity data. Trimetals supported on Al_2O_3 showed poor OCM activity, and the C_2 yield (7.2%) obtained was similar to that of Mn/SiO_2 from this study. Na_2WO_4/MgO, Na_2WO_4/cristobalite and Mn/Na_2WO_4/MgO also show poor OCM activity. The effects of the support on OCM activity clearly suggests that the WO_4 site alone is not the active centre, and that both Na and SiO_2 are involved. The detailed structure of the active site is not clear, but it may involve a distorted tetrahedral Na_2WO_4 closely attached to the α-cristobalite (Na-Si-W-O), as suggested in the literature (Kou *et al.* 1998), with a neighbouring octahedral Mn that increases oxygen transfer ability.

The conditions for the formation of the active site as an efficient catalyst are critical. The restructuring of the surface for the formation of active sites can only occur when W in the form of WO_4 interacts with Si during the phase-transformation process of SiO_2, which is facilitated by Na. The site can only be formed during the in-situ crystallisation process of the silica support. To

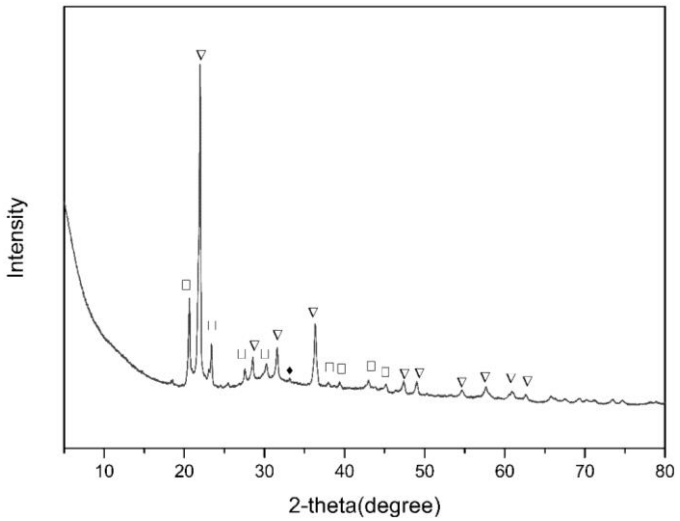

Fig. 7 X-ray diffraction analysis used Mn→Na_2WO_4/SiO_2 catalyst. ▽:α-cristobalite, □:Tridymite, ◆:Mn_2O_3

satisfy this condition, the W must be impregnated on the silica support before or at the same time as Na, followed by a calcination process. The interaction between Na and Mn is not critical, which is confirmed by the impregnation order of Mn and Na_2WO_4 not affecting the activity of trimetallic catalysts.

Fig. 7 plot the XRD of used Mn→Na_2WO_4/SiO_2 catalyst. Compared to the XRD pattern of fresh catalyst (Fig. 4(d)), the α-tridymite peak starts to become more intensive and several peaks ascribed to Na_2WO_4 and Mn_2O_3 were either not detected or less intensive. One of the reason is that the catalyst is diluted by quartz wool during the reaction. The formation of α-tridymite from quartz wool in the presence of Na in the catalyst cannot be avoided. On the other hand, the disappear of those peaks has also been reported in the work of Chua et al, and this was ascribed to the reason that these phases were not stable under persistent OCM reaction environment (Chua *et al.* 2008). The disappear of these phases may cause deactivation of the catalyst, which worth to have further investigation.

5. Conclusions

We have investigated the effect of the individual components, Na, Mn and W, and their combination with SiO_2, on OCM activity. Combinations of Na-Mn, Na-W and Mn-W show strong synergistic effects with a silica support. Na is responsible for the low-temperature crystallisation of silica; however, the crystallisation process is improved in the presence of manganese and tungsten oxide. Manganese oxide exists as Mn_3O_4 in Mn/SiO_2, and the presence of Na promotes the conversion of Mn_3O_4 to Mn_2O_3, independent of the impregnation order of Na and Mn. $MnWO_4$ was detected in the Mn-W combination, which is independent of the impregnation order of Mn and W. However, Na inhibits the formation of $MnWO_4$. Highly dispersed WO_3 was observed in W/SiO_2. The impregnation order of Na and W imparts a dramatic change to the W structure. Na_2WO_4 is observed in the sample in which impregnation of W is followed by Na, while well-dispersed WO_3 is the main phase in the sample with the impregnation order reversed.

Na/SiO_2 and W/SiO_2 showed negligible OCM activity. However, Mn/SiO_2 showed some OCM activity with high oxygen conversion, with the main role of manganese believed to be improving the oxygen transfer during the reaction. The active site for CH_4 activation of $Mn\text{-}Na_2WO_4/SiO_2$ catalyst is related to Na-Si-W-O, and it can only be formed in situ when Na_2WO_4 interacts with silica during its crystallisation facilitated by Na.

References

Arndt, S., Otremba, T., Simon, U., Yildiz, M., Schubert, H. and Schomackera, R. (2012), "$Mn\text{-}Na_2WO_4/SiO_2$ as catalyst for the oxidative coupling of methane what is really known?", *Appl. Catal. A*, **425**, 53-61.

Chang, Y.F. and McCarty, J.G. (1996), "Novel oxygen storage components for advanced catalysts for emission control in natural gas fueled vehicles", *Catal. Today*, **30**(1-3), 163-170.

Chua, Y.T., Mohamed, A.R. and Bhatia, S. (2008), "Oxidative coupling of methane for the production of ethylene over sodium-tungsten-manganese-supported-silica catalyst ($Na\text{-}W\text{-}Mn/SiO_2$)", *Appl. Catal. A*, **343**(1), 142-148.

Czuprat, O., Schiestel, T., Voss, H. and Caro, J. (2010), "Oxidative coupling of methane in a BCFZ perovskite hollow fiber membrane reactor", *Ind. Eng. Chem. Res.*, **49**(21), 10230-10236.

Elkins, T.W. and Hagelin-Weaver, H.E. (2015), "Characterization of $Mn\text{-}Na_2WO_4/SiO_2$ and $Mn\text{-}Na_2WO_4/MgO$ catalysts for the oxidative coupling of methane", *Appl. Catal. A*, **497**, 96-106.

Fleischer, V., Steuer, R., Parishan, S. and Schomäcker, R. (2016), "Investigation of the surface reaction network of the oxidative coupling of methane over $Na_2WO_4/Mn/SiO_2$ catalyst by temperature programmed and dynamic experiments", *J. Catal.*, **341**, 91-103.

Gao, W.W., Ye, S.Y. and Shao, M.W. (2011), "Solution-combusting preparation of mono-dispersed Mn_3O_4 nanoparticles for electrochemical applications", *J. Phys. Chem. Sol.*, **72**(9), 1027-1031.

Gordienko, Y., Usmanov, T., Bychkov, V., Lomonosov, V., Fattakhova, Z., Tulenin, Y., Shashkin, D. and Sinev, M. (2016), "Oxygen availability and catalytic performance of $NaWMn/SiO_2$ mixed oxide and its components in oxidative coupling of methane", *Catal. Today*, **278**, 127-134.

Hou, S.C., Cao, Y., Xiong, W., Liu, H.C. and Kou, Y. (2006), "Site requirements for the oxidative coupling of methane on SiO_2-supported Mn catalysts", *Ind. Eng. Chem. Res.*, **45**(21), 7077-7083.

Ji, S.F., Xiao, T.C., Li, S.B., Chou, L.J., Zhang, B., Xu, C.Z., Hou, R.L., York, A.P.E. and Green, M.L.H. (2003), "Surface WO_4 tetrahedron: The essence of the oxidative coupling of methane over $M\text{-}W\text{-}Mn/SiO_2$ catalysts", *J. Catal.*, **220**(1), 47-56.

Ji, S.F., Xiao, T.C., Li, S.B., Xu, C.Z., Hou, R.L., Coleman, K.S. and Green, M.L.H. (2002), "The relationship between the structure and the performance of $Na\text{-}W\text{-}Mn/SiO_2$ catalysts for the oxidative coupling of methane", *Appl. Catal. A*, **225**(1), 271-284.

Jiang, Z.C., Yu, C.J., Fang, X.P., Li, S.B. and Wang, H.L. (1993), "Oxide/support interaction and surface reconstruction in the Na_2WO_4/SiO_2 system", *J. Phys. Chem.*, **97**(49), 12870-11287.

Jones, C.A., Leonard, J.J. and Sofranko, J.A. (1987), "The oxidative conversion of methane to higher hydrocarbons over alkali-promoted Mn/SiO_2", *J. Catal.*, **103**(2), 311-319.

Kou, Y., Zhang, B., Niu, J.Z., Li, S.B., Wang, H.L., Tanaka, T. and Yoshidac, S. (1998), "Amorphous features of working catalysts: XAFS and XPS characterization of $Mn/Na_2WO_4/SiO_2$ as used for the oxidative coupling of methane", *J. Catal.*, **173**(2), 399-408.

Mahmoodi, S., Ehsani, M.R. and Ghoreishi, S.M. (2010), "Effect of promoter in the oxidative coupling of methane over synthesized Mn/SiO_2 nanocatalysts via incipient wetness impregnation", *J. Ind. Eng. Chem.*, **16**(6), 923-928.

Nipan, G.D., Buzanov, G.A., Zhizhin, K.Y. and Kuznetsov, N.T. (2016), "Phase states of

Li(Na,K,Rb,Cs)/W/Mn/SiO_2 composite catalysts for oxidative coupling of methane", *Russ. J. Inorg. Chem.*, **61**(14), 1689-1707.

Noon, D., Seubsai, A. and Senkan, S. (2013), "Oxidative coupling of methane by nanofiber catalysts", *ChemCatChem*, **5**(1), 146-149.

Palermo, A., Vazquez, J.P.H. and Lambert, R.M. (2000), "New efficient catalysts for the oxidative coupling of methane", *Catal. Lett.*, **68**(3-4), 191-196.

Palermo, A., Vazquez, J.P.H., Lee, A.F., Tikhov, M.S. and Lambertz, R.M. (1998), "Critical influence of the amorphous silica-to-cristobalite phase transition on the performance of Mn-Na_2WO_4/SiO_2 catalysts for the oxidative coupling of methane", *J. Catal.*, **177**(2), 259-266.

Pol, V.G., Gedanken, A. and Calderon-Moreno, J. (2003), "Deposition of gold nanoparticles on silica spheres: A sonochemical approach", *Chem. Mater.*, **15**(5), 1111-1118.

Ren, Y., Bruce, P.G. and Ma, Z. (2011), "Solid-solid conversion of ordered crystalline mesoporous metal oxides under reducing atmosphere", *J. Mater. Chem.*, **21**(25), 9312-9318.

Senthil, K. and Yong, K. (2007), "Growth and characterization of stoichiometric tungsten oxide nanorods by thermal evaporation and subsequent annealing", *Nanotechnol.*, **18**(39), 1-7.

Serres, T., Aquino, C., Mirodatos, C. and Schuurman, Y. (2015), "Influence of the composition/texture of Mn-Na-W catalysts on the oxidative coupling of methane", *Appl. Catal. A*, **504**, 509-518.

Sharma, B.K. (1997), *Industrial Chemistry (Including Chemical Engineering)*, Goel Publishing House, Meerut, India.

Simon, U., Gorke, O., Berthold, A., Arndt, S., Schomacker, R. and Schubert, H. (2011), "Fluidized bed processing of sodium tungsten manganese catalysts for the oxidative coupling of methane", *Chem. Eng. J.*, **168**(3), 1352-1359.

Stobbe, E.R., De Boer, B.A. and Geus, J.W. (1999), "The reduction and oxidation behaviour of manganese oxides", *Catal. Today*, **47**(1-4), 161-167.

Wang, D., Rosynek, M.P. and Lunsford, J.H. (1995), "Oxidative coupling of methane over oxide-supported sodium-manganese catalysts", *J. Catal.*, **155**(2), 390-402.

Wu, J.A. and Li, S.B. (1995), "The role of distorted WO_4 in the oxidative coupling of methane on tungsten oxide supported catalysts", *J. Phys. Chem.*, **99**(13), 4566-4568.

Wu, J.G., Li, S.B., Niu, J.Z. and Fang, X.P. (1995), "Mechanistic study of oxidative coupling of methane over $Mn_2O_3/Na_2WO_4/SiO_2$ catalyst", *Appl. Catal. A*, **124**(1), 9-18.

Zhang, H.L., Wu, J.J., Qin, S. and Hu, C.W. (2006), "Study of the effect of gas space time on the combination of methane gas-phase oxidation and catalytic oxidative coupling over $Mn/Na_2WO_4/SiO_2$ catalyst", *Ind. Eng. Chem. Res.*, **45**(21), 7090-7095.

Zhao, Q.F., Chen, S.L., Gao, J.S. and Xu, C.M. (2009), "Effect of tungsten oxide loading on metathesis activity of ethene and 2-butene over WO_3/SiO_2 catalysts", *Transit. Met. Chem.*, **34**(6), 621-627.

CC